

Time-resolved CARS measurements of vibrational decoherence of I_2 isolated in matrix Ar

M. Karavitis, D. Segale, Z. Bihary, M. Pettersson, and V.A. Apkarian

Department of Chemistry, University of California Irvine, CA 92697-2025, USA

E-mail: aapkaria@uci.edu

Time-resolved coherent anti-Stokes Raman scattering is applied to prepare and interrogate vibrational coherences on the ground electronic surface of molecular iodine isolated in Ar matrices. The coherence decay time shows a linear dependence on vibrational quantum numbers, for $v = 3-15$. The temperature dependence of decoherence rates is negligible for $v < 7$, in the experimental range $T = 18-32$ K. For a $v = 13, 14$ superposition, the temperature dependence indicates dephasing by a 66 cm^{-1} pseudo-local phonon, just outside the Debye edge of the solid. The accuracy of the data is limited due to two-photon induced dissociation of the molecule, which process is characterized using polarized fields. The $T \rightarrow 0$ limit of dephasing is discussed.

PACS: 42.65.Dr, **67.80.-s**

1. Introduction

In a recent paper, we reported time-resolved coherent anti-Stokes Raman scattering (TRCARS) measurements on I_2 isolated in matrix Ar [1]. A detailed analysis of the process was presented, based on data limited to wavepackets prepared near $v = 4$, and limited to $T = 32$ K. We have, since, succeeded in making measurements on packets prepared at vibrations as high as $v = 14$, and as a function of temperature, for $T = 17-33$ K. TRCARS measurements are well suited for the preparation of vibrational coherences, and the detailed analysis of their dephasing [2,3]. The characterization of vibrational decoherence in this model system: a diatomic impurity, in an atomic solid, with weak and relatively well understood coupling between molecule and lattice [4], is our aim. Of particular interest is the understanding of decoherence in the $T \rightarrow 0$ limit [5].

Studies of vibrational relaxation and dephasing dynamics in cryogenic matrices are limited for the most part to infrared active diatomics, such as CO, in which in the $T \rightarrow 0$ limit radiative relaxation or dipolar intermolecular energy transfer remains as the residual source of dephasing [6]. These mechanisms are not available to a homonuclear diatomic, which now must be prepared via Raman pumping. Raman lineshapes, in principle, yield overall dephasing rates; however, practical considerations do not allow studies with the required resolution [7]. TRCARS measurements allow the preparation of vibrational coherences

with control, and allow a detailed time domain interrogation of their evolution.

Argon matrices doped with molecular iodine prove to be difficult to scrutinize, because the signal permanently degrades during the course of measurement. We establish that the degradation is due to permanent dissociation of the molecule through multi-photon excitation, a process unavoidable at the field strengths required for the four-wave mixing measurements. Despite this limitation, important principles are established.

2. Experimental

A detailed description of the experimental method can be found in our earlier report [1]. Succinctly, the forward BOXCARS geometry is adopted, using three noncollinear laser pulses at two different colors [8]. The pulses are obtained from a regeneratively amplified Ti:sapphire laser, which pumps two three-pass optical parametric amplifiers (OPA). The OPA outputs are up-converted by sum frequency generation, and compressed using prism-pairs to provide independently tunable ~ 70 fs pulses in the range 480 nm to 2000 nm. Using a neutral density filter, the intensities of the lasers are separately attenuated to less than $1 \mu\text{J}/\text{pulse}$. The three horizontally polarized input beams are brought into focus on the sample through a single achromat. A pinhole is used to spatially filter the anti-Stokes (AS) output beam. Spectral filtering is provided with a combination of a bandpass filter

and 1/4-m monochromator, adjusted to pass the entire band of the AS radiation. The signal is detected using a photomultiplier. Typically, 300 averages are taken at each time-delay. Data was also collected with a laser system consisting of two home-build noncollinear optical parametric amplifiers, capable of generating 25 fs pulses at the sample.

The matrices are deposited at 32 K, using a pulsed valve (General Valve, Series 99) from a 5-liter glass bulb, onto a 200- μm thick sapphire substrate. The substrate is cooled using a closed-cycle cryostat, which in these experiments could only reach a base temperature of 17 K. The cryostat is mounted on an x - y - z translation stage. The deposition conditions are adjusted to obtain a glassy film of high optical quality. A back pressure of ~ 200 Torr and long pulses of ~ 1 s, consistently yield films of sufficient quality for the measurements. Using a scanning pinhole, the spot size at the overlap of the three laser beams is measured to have a typical diameter of FWHM = 35 μm . This is comparable to the grain size of crystallites, as such the measurements can be expected to be confined to single, oriented, crystalline domains. This consideration is also key to our success in carrying out temperature dependent measurements, despite the fact that the thermal shock of cooling leads to shattering of the solid. In the shattered solids, a careful search usually allows us to find a scatter-free domain to carry out the measurements.

At a given spot, the signal undergoes radiation induced permanent decay. The signal recovers upon moving to a fresh spot. Inspection of the irradiated volume under magnification establishes that the decay is not due to physical damage of the sample. Since the TRCARS experiments are carried out with all three input beams horizontally polarized, irradiation-induced re-orientation of the molecular axis could lead to signal decay. To test this hypothesis, we insert a half-wave plate in one of the pump beams to rotate its polarization by 90°. After passing the two pump beams through a cross-oriented pair of linear polarizers we overlap the beams in space and time by optimizing the CARS signal from the sapphire substrate. We then translate the sample to the focal plane, and verify that the two-photon induced molecular fluorescence at 1340 nm is proportional to the square of the sum of intensities of the beams. The sample is then irradiated on the same spot alternatively with the horizontally and vertically polarized pump beams, by blocking and unblocking beams while monitoring two-photon induced fluorescence previously assigned to $\text{I}^*\text{I}^* \rightarrow \text{I}^*\text{I}$ emission [9].

3. Results and analysis

3.1. Photodissociation

The decay of the laser induced molecular emission with irradiation time is shown in Fig. 1, for a sequence of irradiation periods alternating between vertically and horizontally polarized beams. The intensities of the two beams were adjusted to provide equal signal from each beam when irradiating a fresh spot. The decay curve for a given polarization is nonexponential. Upon switching from vertical to horizontal irradiation of the same spot, the fluorescence intensity jumps up, however it starts below the pre-irradiation level. Evidently, irradiation leads to dissociation of molecules oriented both parallel and perpendicular to the polarization of the laser. After irradiation with the horizontal polarization, when we return back to the vertical polarization we observe a small increase above the limit reached in the first irradiation period. We may conclude that a small fraction of the molecules re-orient, or that a small fraction of the previously dissociated molecules recombine. The same decay behavior is obtained when monitoring various molecular emissions: the ion-pair emission at 380 nm [10–12], the I^*I^* emission in the near IR [9], and the $A/A' \rightarrow X$ emission near 1400 nm [13,14]. Since all molecular emissions decay in time, we may safely conclude that the molecule dissociates.

The decay curves at three different irradiation intensities are shown in Fig. 2. The curves are not exponential, and not expected to be. For molecules rigidly

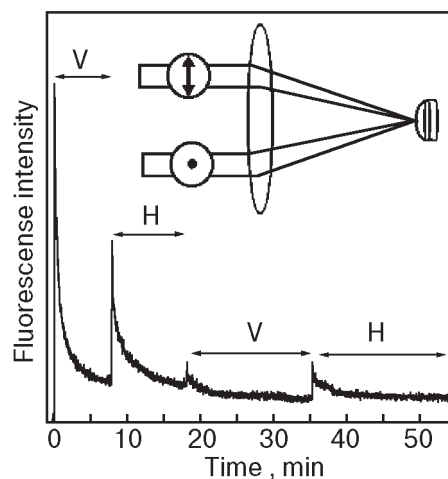


Fig. 1. Photoinduced dissociation of molecular iodine, monitored using two-photon fluorescence at 1340 nm. The experimental arrangement is shown. Two cross-polarized laser beams ($\Delta t = 50$ fs near transform limited pulses, $\lambda = 555$ nm, 1 kHz repetition rate) are aimed at the same spot in the sample. The sample is irradiated successively with the vertical (V) and horizontal (H) polarized beams over the durations indicated by the double-sided arrows.

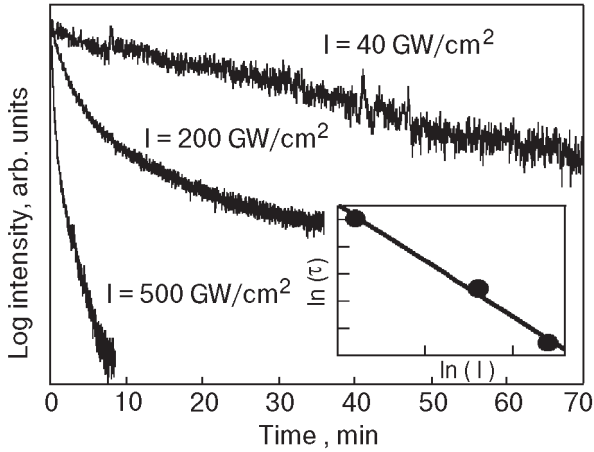


Fig. 2. Decay of I_2 fluorescence as a function of pump intensity. Experimental conditions are identical to those described in Fig. 1. Differing intensities are produced by means of a variable neutral density filter with a continuous range of optical densities between 0.02 and 3 arb. units. The inset shows a log/log plot of the decay rate vs. the pump intensity. The result is a straight line of slope two, indicating that the dissociative excitation is via two-photon absorption.

held by the matrix, such that their orientations do not scramble during irradiation, photodissociation with polarized light leads to orientation dependent population decay. The kinetics and observable signal will be controlled by the tensor of molecular transition matrix elements involved in the dissociative transition and probe transitions. This occurs in studies of saturation of photo-selection or induced dichroism, and many of the common cases that arise have been reviewed in the literature [15]. For the present purposes we note that the signal can be approximated by a double exponential, with decay constants at a given intensity that differ by a factor of 10. Both decay constants scale as the second power of the intensity, as illustrated for the fast component in the inset to Fig. 2. This suggests that the dissociation is due to two-photon excitation, with the two decay rates assigned to photo-dissociation of molecules oriented parallel and perpendicular to the linearly polarized radiation field. Thus, for irradiation with x -polarized light, identifying the two-photon excitation cross-sections as $\sigma_{\parallel}^{(2)}$ and $\sigma_{\perp}^{(2)}$, and associating a quantum yield Q for dissociation upon excitation, the observable signal may be approximated as:

$$N(t) = \frac{N_0}{3} \left[\zeta_{\parallel} \exp(-\sigma_{\parallel}^{(2)} I_x^2 Q t') + 2\zeta_{\perp} \exp(-\sigma_{\perp}^{(2)} I_x^2 Q t') \right], \text{ where } t' = ft\Delta t \quad (1)$$

in which ζ_{\parallel} and ζ_{\perp} are the sensitivities of LIF detection of the parallel and perpendicular populations, I

is the laser fluence in photons $\text{cm}^{-2}\cdot\text{s}^{-1}$, Δt is the laser pulse width, f is the laser repetition rate (1 kHz), and t is the irradiation duration.

The lower limit for the two-photon excitation cross-section that leads to dissociation can be obtained by assuming $Q = 1$, in which case the fits yield $\sigma_{\parallel}^{(2)} = 2 \cdot 10^{-51} \text{ cm}^4 \cdot \text{s}$ and $\sigma_{\perp}^{(2)} = 2 \cdot 10^{-52} \text{ cm}^4 \cdot \text{s}$. The largest error in the determination of these limiting values is the uncertainty associated with the measured spot size of the laser.

The upper limit of the two-photon excitation cross-section can be obtained under the assumption that beside the linear $B \leftarrow X$ absorption, this process dominates the attenuation of the pump laser, in which case the transmitted intensity I reduces to:

$$I = I_0 / (1 + 2N\sigma^{(2)}I_0l) \quad (2)$$

in which $N = 4 \cdot 10^{18} \text{ cm}^{-3}$ is the dopant number density, and $l \sim 50 \mu\text{m}$ is the sample thickness. From the curvature of the transmission, for pump intensities limited to $0.5 \mu\text{J}/\text{pulse}$, we measure $\sigma^{(2)} = 10^{-48} \text{ cm}^4 \cdot \text{s}$. The sample thickness is the greatest uncertainty in this determination.

3.2. Time-resolved CARS

The TRCARS measurements are designed to interrogate the vibrational coherence on the ground electronic state of matrix isolated iodine. The experiments measure a single component of the third order polarization:

$$P_{\mathbf{k}_1 - \mathbf{k}_2 + \mathbf{k}_3}^{(0,3)}(t) = \langle \varphi^{(0)}(t) | \hat{\mu} | \varphi_{\mathbf{k}_1 - \mathbf{k}_2 + \mathbf{k}_3}^{(3)}(t) \rangle + \text{c.c.} \quad (3)$$

by detecting the AS radiation propagating in the $\mathbf{k}_1 - \mathbf{k}_2 + \mathbf{k}_3$ direction [1]. We detect the total AS radiation:

$$I_{\text{CARS}}(t) = \int_{-\infty}^{\infty} dt_{43} \left| P^{(3)}(t_{21}, t_{32}, t_{43}) \right|^2 \quad (4)$$

which depends on the timing between the sequence of three pulses: t_{21} is the interval between pump and dump, t_{32} is the interval between dump and probe, and t_{43} is the radiation interval after arrival of the probe pulse. In all of the measurements to be reported, the pump and dump pulses are stationary and nearly coincident in time. Their delay, t_{21} , is adjusted for optimum signal. Due to fast electronic dephasing, only prompt radiation after arrival of the probe pulse contributes to the signal, $t_{43} < 30 \text{ fs}$. This time interval is fixed by the first arrival of $\varphi^{(3)}$ to the inner turning point of the excited electronic surface, where the energy conservation condition $\omega_{\text{AS}} = \omega_1 - \omega_2 + \omega_3$ can be met. Consistent with this, the AS spectrum is

verified to be structureless. We adjust the spectral bandpass of the detection to accept the entire AS spectrum. The signal is then recorded as a function of t_{32} , namely, as a function of delay between the preparation of the Raman packet, $\varphi_{\mathbf{k}_1-\mathbf{k}_2}^{(2)}$, and the arrival of the probe pulse at t_3 . Thus, by defining $t \equiv t_{32}$, it is made clear that the experiment measures the time correlation between the Raman packet and the zeroth order initial state:

$$I_{CARS}(t) \propto \left| 2\text{Re} \left\langle \varphi^{(0)}(t_{32}) \left| \varphi_{\mathbf{k}_1-\mathbf{k}_2}^{(2)}(t_{32}) \right. \right\rangle \right|^2. \quad (5)$$

The decay of this correlation defines the vibrational decoherence (permanent dephasing).

With laser intensities limited to <100 nJ per pulse, the sample degradation time stretches sufficiently to allow meaningful measurements. From a given spot, we record waveforms in pairs. After scanning a particular delay between pulses, we retrace the scan. An example is shown in Fig. 3. In this case, upon retracing, the signal recovers to 10% of its original amplitude over the data acquisition time of 20 minutes. This information is used to correct for signal degradation. In the TRCARS measurements, all three input beams are polarized parallel to each other, therefore the quadrilinear signal is from the population oriented along the polarization axis, $N_{\parallel}(t)$. As long as the decay of this sub-ensemble is not too extensive, it is possible to approximate it as an exponential. Accord-

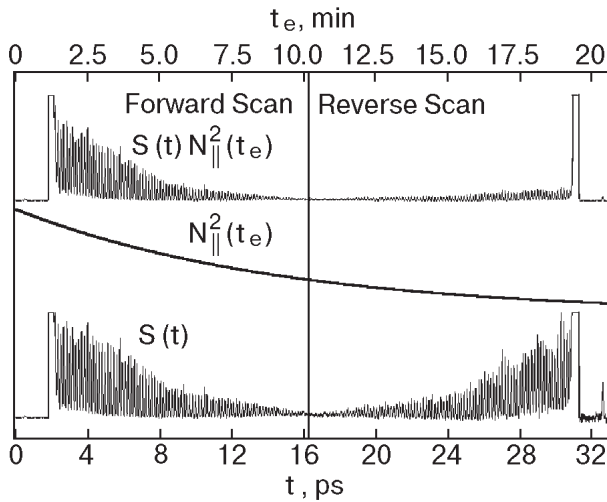


Fig. 3. Forward and reverse scans of the TRCARS signal. Overlapping ~ 25 fs pump and Stokes pulses (at $\lambda = 529$ and 575 nm) are used to generate a wavepacket on the X state centered on $v = 4, 5$. The lower abscissa is the delay time between Stokes and probe pulse, while the upper abscissa is the data acquisition time. Around 10 percent of the original signal is recovered over the entire scan. An exponential correction, N_{\parallel}^2 has been introduced in the final signal, $S(t)$, in order to account for sample degradation over the course of the experimental time (t_e).

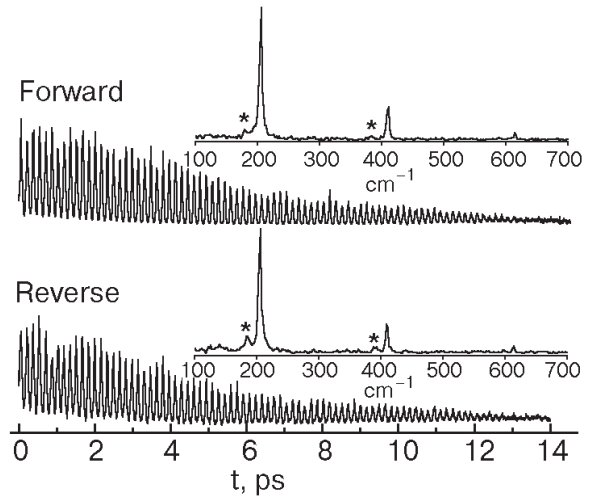


Fig. 4. Corrected CARS signal obtained using pulses described in Fig. 3. The insets are the Fourier transforms of the corresponding time files. The fundamental beat ~ 200 cm^{-1} along with two overtones, are a clear indication of a four state superposition. The Stokes shift, centered at 1475 cm^{-1} would support a wavepacket centered around a 7, 8 superposition; however, nonlinear least squares analysis of this signal using Eq. (7) yield frequencies corresponding to a 5, 6, 7, 8 superposition. This is not unreasonable considering the FWHM of the pulses used in these experiments is greater than 800 cm^{-1} .

ingly, the signal, which is proportional to $N_{\parallel}^2(t)$, is corrected for exponential degradation with measurement time. The reconstruction of the signal is shown in Fig. 3.

In Fig. 4 we show the signal from a sample deposited at 35 K and recorded at 17 K. Both forward and corrected backward scans are shown. The good comparison between the two scans is a measure of the adequacy of the correction: the distortion of the signal due to nonexponential degradation, is minor. The Fourier transforms of the two time files, which are also shown, are in good agreement. Thus, information regarding the complex amplitudes of the vibrational superposition and their beat frequencies is rather reliable, while dephasing times are subject to the uncertainty introduced by the correction for signal degradation. This data set was obtained using the short pulse NOPA setup, with pulse widths of ~ 25 fs. The observation of the fundamental beat, $\Delta v = 1$ at 205.5 cm^{-1} , and two overtone beats, $\Delta v = 2$ and $\Delta v = 3$, indicates that a superposition of four vibrational levels is prepared. Given the Stokes shift of 1500 cm^{-1} between pump and dump pulses, the superposition is centered near $v = 7$. Additionally, a broad side-band to the red of the molecular lines can be seen (identified by asterisks in Fig. 4). The fundamental beat of 180 cm^{-1} identifies this sideband as the dimer [16]. It is noteworthy that the dimer band is sharper during the

backward scan, indicating annealing of the spot during the course of the measurement. The molecular lines do not show a discernible annealing effect. In samples deposited at $T < 32$ K, the dimer is not observed.

Ignoring time convolution of the probe window with the evolving coherence, and acknowledging that sum beats are outside the time resolution of the measurement, the signal is analyzed as a sum of decaying sinusoids:

$$S(t) = \sum_v c_v^2 e^{-2\gamma_v t} + \sum_{v,v' \neq v} c_v c_{v'} \cos[(\omega_v - \omega_{v'})t + (\varphi_v - \varphi_{v'})] e^{-(\gamma_v + \gamma_{v'})t} \quad (6)$$

in which γ , c , and φ represent the overall dephasing rate, amplitude, and phase of a given vibrational state of the prepared superposition. Using the Fourier analysis for initial estimates, the time files are fit through a nonlinear regression to Eq. (6). Although an excellent reproduction of the signal is retrieved, due to the relatively short time file, the individual decay constants of the constituent states are not separately determined. An equally acceptable fit of the time file is obtained by setting all decay constants to be the same, $1/\gamma = 4.2$ ps in this particular case. In this regard, the use of longer pulses (narrower bandwidth) for the preparation of the Raman packet is

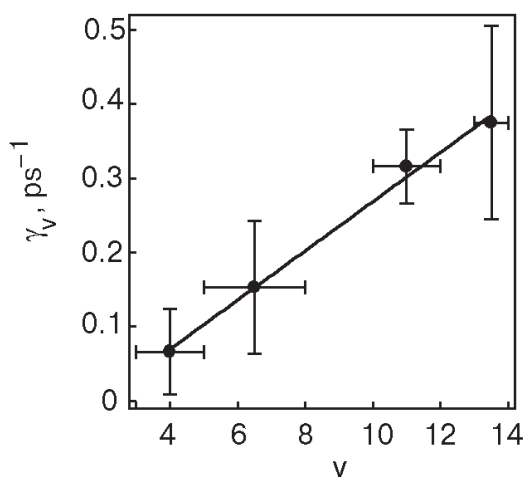


Fig. 5. Dependence of dephasing on vibrational quantum number. The four dephasing rates shown in the figure correspond to the following superpositions: (3,4,5), (5,6,7,8), (10,11,12) and (13,14). Due to the short lifetimes of these superpositions relative to the anharmonicity, the individual dephasing rates could not be decoupled from each other; therefore, only the mean dephasing rates are used. Error bars on the v axis span the superposition while error bars on the γ_v axis correspond to the standard deviation of the mean dephasing rates obtained from a nonlinear least squares fit to the data.

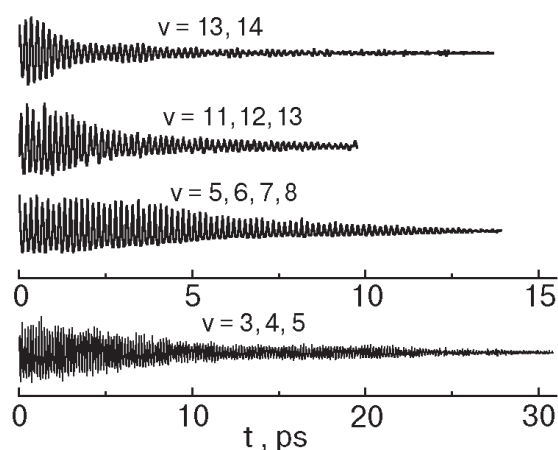


Fig. 6. Experimental waveforms corresponding to vibrational levels ranging from $v = 3$ to $v = 14$. These signals have their zero frequency components subtracted out in order to make meaningful comparisons. Some important features of these signals include the nodal patterns exhibited by the 3, 4, 5 and the 13, 14 superpositions. The node in the 3, 4, 5 superposition, ~ 13 ps, corresponds to a rephasing time associated with twice the anharmonicity indicating that at least four states must be contributing to this signal even though only three were resolvable. The slow modulation of the signal with a period of 25 ps in the $v = 13, 14$ superposition is too short to be associated with anharmonicity.

preferable, since this allows a better discrimination of the v -dependence of γ . The extracted values of γ are collected in Fig. 5, in which the horizontal error bars highlight the fact that individual dephasing rates cannot be decoupled with confidence. The dependence is linear, with $1/\gamma$ varying from 16 ps to 2.7 ps for $v = 3$ to $v = 13$. A representative set of waveforms from which the dephasing rates were extracted, is shown in Fig. 6. Based on the used Stokes shifts, $\omega_{\text{pump}} - \omega_{\text{dump}}$, the assignment of the prepared vibrations can be made with little ambiguity. The analysis provides a rather accurate determination of vibrational frequencies and anharmonicities, as shown in Fig. 7. The extracted harmonic frequency, and anharmonicity are: $\omega_e = (214.0 \pm 0.17) \text{ cm}^{-1}$, $\omega_e x_e = (0.638 \pm 0.009) \text{ cm}^{-1}$. These values are in good agreement with the RR measurements in solid Ar [7], and are somewhat revised from our earlier report. Note, the superposition with the lowest vibrations assigned to $v = 3, 4, 5$ in Fig. 6, lives long enough to show a weak node near $t = 13$ ps, which arises from the anharmonic beat between $\omega_{43} - \omega_{65} = 4\omega_e x_e$ indicating that the superposition contains $v = 6$ as well. The node between neighboring beats occurs at $t = c/2\omega_e x_e = 26$ ps, by which time the signal is quite weak.

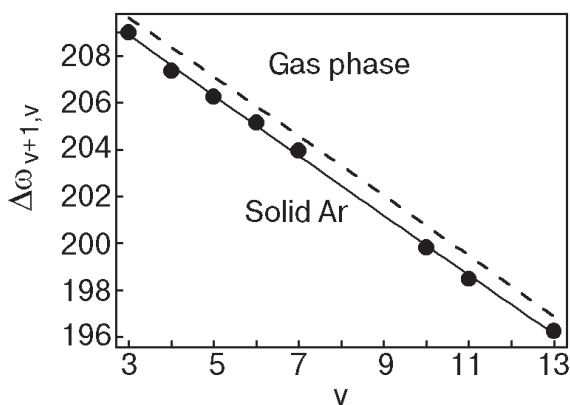


Fig. 7. Birge-Spinner plot for gas phase I_2 (dashed line), and I_2 in solid Ar obtained in the present TRCARS measurements (filled circles). The circles represent the experimental data points. The fundamental frequency as well as the first anharmonicity are slightly modified from the gas phase values and in agreement within experimental error to those obtained from resonance Raman.

Within the accuracy of the measurements, for packets prepared below $v = 10$, the decoherence rates are insensitive to temperature in the experimental range of $T = 17$ – 32 K. Temperature has a measurable effect on the $v = 13, 14$ packet. This is illustrated in Fig. 8, in which the time files along with the spectra of the fundamental beat are shown. The spectra reveal sidebands at 10 cm^{-1} flanking the main peak. This, in the time profile leads to the 3 ps modulation (see 17 K signal in Fig. 8), which cannot be confused with the anharmonicity beat. The spectrum clearly shows that while the lines broaden with temperature, such that in the 33 K spectrum the sidebands have completely coalesced with the central peak. The dephasing times extracted from transients through the least squares regression are: $1/\gamma = 4$ ps, 3.6 ps, and 2.9 ps at $T = 17, 25$, and 33 K, respectively. For the lower vibrations,

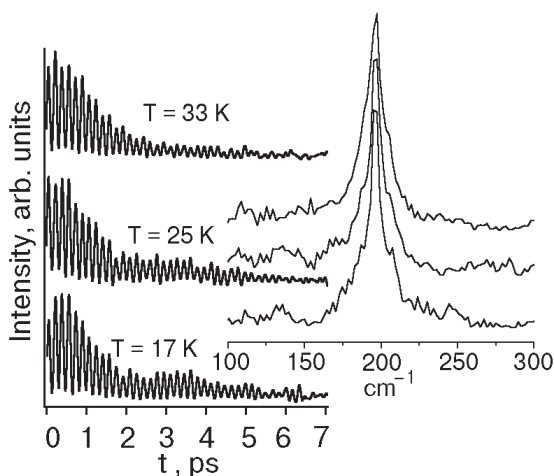


Fig. 8. Decoherence rates for different temperatures.

in the same temperature range, the T -dependence is less than 10%.

4. Discussion

In molecular systems, with many internal degrees of freedom, the preparation and interrogation of particular coherences will be limited by competition among different channels. The dense electronic manifold of iodine leads to multiple electronic excitation channels at the intensities required to drive nonlinear processes. The time dependence of the four-wave signal is impervious to background excitation channels, except for the photodissociation of the molecule. Since the photodissociation process is two-photon driven, while the four-wave mixing process is maintained in the quadrilinear regime, it cannot be prevented through intensity control. Since the electronic resonances involved in both the TRCARS and multi-photon excitation involve repulsive walls of potentials, they are broad, and color offers little selectivity over the branching. Indeed, dissociation occurs at all colors used in the TRCARS experiments. Let us put the measured cross-sections in perspective. The $B \leftarrow X$ excitation cross-section is $\sigma_{BX} = 10^{-18} \text{ cm}^2$ ($|\mu_{BX}|^2 = 1.02 \text{ D}^2$ at 550 nm) [17]. The cross-section associated with the bilinear stimulated Raman process for preparing the vibrational coherence in the X state can be estimated as $\sigma_{SR}^{(2)} = \sigma_{XB}\sigma_{BX}\Delta\tau = 2 \cdot 10^{-50} \text{ cm}^4 \cdot \text{s}$, where $\Delta\tau \sim 20$ fs is the residence time of the B -state packet in the Franck-Condon window. The measured two-photon induced dissociation cross-section is $\sigma_{\parallel}^{(2)}Q = 2 \cdot 10^{-51} \text{ cm}^4 \cdot \text{s}$, only an order of magnitude smaller. Therefore, for a given number density transferred to the Raman packet, a tenth undergo permanent dissociation. The reduction of intensities to minimize the fraction of molecules that dissociate during the course of measurement is limited by practical signal-to-noise considerations. At intensities of 100 nJ/pulse ($10^{29} \text{ photons/cm}^2 \cdot \text{s}$), 10 ppm of the molecules are transferred to the Raman packet, and the third order polarization consists of $\sim 10^4$ molecules, leading to ~ 1 CARS photon detected per pulse.

The permanent photo-dissociation of iodine in solid argon is of interest, especially since this system has been previously studied as a prototype for the perfect cage effect [18]. A detailed analysis of the process will be taken up elsewhere. Here, we suffice by recognizing that permanent dissociation, as opposed to molecular re-orientation takes place during the measurements. The polarization dependent measurement clearly shows that early dissociation will result in orientational anisotropy, therefore dichroism in the solid. The neglect of this consideration can have significant consequences on the interpretation of photo-selection,

or photo-bleaching experiments such as have been reported recently [12]. Upon extended irradiation, the entire population is depleted. Although this would occur even if the molecule only possessed a single transition dipole, careful analysis of the decay establishes that the process is bimodal, both perpendicular and parallel molecular orientations undergo two-photon dissociation with relative yields of $\sigma_{\parallel}^{(2)}/\sigma_{\perp}^{(2)} = 10$. Assuming quantum yields independent of orientation, the ratio must be determined by the relative excitation cross-sections. There are two electronic states, $B(0_u)$ and $B'(1_u)$, that serve as intermediates for resonant two-photon excitation in the spectral range of interest. The $B \leftarrow X$ transition dipole is parallel to the molecular axis ($\Delta\Omega = 0$), while the $B' \leftarrow X$ transition is perpendicular to the molecular axis ($\Delta\Omega = \pm 1$); moreover, at the measured wavelength of 550 nm the relative absorption cross-sections of these transitions have a ratio of 9:1 [17]. This, nicely rationalizes the observed orientation dependence of the dissociation curves, with the added implication that the two-photon cross-sections are principally determined by the initial resonance.

Our main interest in the present work is the description of vibrational dephasing in the low temperature limit. The observable vibrational coherence will decay due to dissipation and pure dephasing due to homogeneous and inhomogeneous contributions. In addition, there can be a contribution due to the preparation. We consider the signatures of each of these processes, focusing only on the most robust features of the data. Our prior theoretical analysis of the I_2/Ar system, using vibrational self-consistent field (VSCF) for the analysis of anharmonic modes, their couplings, and the expected effect on TRCARS observables serves as a backdrop for this discussion [4].

In electronically resonant CARS, the preparation of the Raman packet entails evolution on the electronically excited state. Although this evolution is limited in time to the arrival of the packet into the Stokes window, 10–30 fs depending on the Stokes shift, it will nevertheless impart momentum to lattice coordinates that are coupled through the electronic transition (electron-phonon coupling). Feedback following this impulsive drive should occur on the time scale of the characteristic local phonon periods, $0.5 \text{ ps} > \tau > 2 \text{ ps}$. Careful inspection of the envelopes of the time profiles of the signals reveals such modulations at early time. To uniquely assign and characterize the effect of impulsive momentum kicks, a more systematic set of accurate measurements is desirable.

Two important inhomogeneous sources of dephasing were considered explicitly in Ref. 4. The first of these recognizes that at finite temperature, the initial

state, $\phi^{(0)} = |v=0, \{n_i(T)\}\rangle$ consists of the chromophore in $v=0$, and a thermal distribution of phonon occupation numbers, n_i . On the preparation time scale, save for the momentum kicks imparted to selected modes, the phonon distribution is frozen. Due to the statistical distribution of initial phases in the coupled modes, the system will dephase even if the phonons are harmonic. This will contribute a temperature dependent inhomogeneous mechanism for dephasing, which is linear in vibrational quantum number due to the linear dependence of the anharmonic coupling on v . Although we see a linear dependence of dephasing rates on v , the only measurable temperature dependence occurs at $v = 13, 14$. A vibration specific temperature dependence is not consistent for this mechanism, suggesting that this contribution is small. A second important inhomogeneous contribution can be expected from lattice defects. The explicit model considered was that of vacancy point defects. Due to the anharmonic coupling between chromophore and vacancies, this mechanism also leads to dephasing rates linear in vibrational quantum number. Moreover, due to the bimodal distribution of vacancy induced frequency shifts, the model predicts sidebands in the spectrum and accordingly, modulation on the envelope of the signal. The predicted observable TRCARS signal for a $v = 10, 11$ packet (Fig. 7 of Ref. 4) is in surprisingly good agreement with the $v = 13, 14$ packet observed in Fig. 8. Sidebands separated by 12 cm^{-1} , which coalesce with the central peak between $T = 15$ and 35 K , was predicted there, as is observed here. This is the origin of the 2.5 ps modulation of the time domain signal. The assumed vacancy concentration in the model was 1.4 %. Since the depth of modulation of the signal is also in quantitative agreement with the model, we must conclude that the defect concentration is comparable in the experiment. Small sidebands, which appear as pedestals in the Fourier spectra (see spectra in Fig. 4) are often observed with varying amplitude, consistent with the expectation that defect concentrations may vary with preparation, and with the selected spot in a given film. Although the films are polycrystalline, the measurement is carried out in selected $\sim 50 \mu\text{m}$ spots that may also contain grain boundaries, hence unusual densities of defects.

The observation of dephasing rates linear in vibrational quantum number is consistent with the fact that the coupling between the molecular vibrations and lattice phonons is weak. Then spectral shifts and dephasing rates will be mediated through the lowest order anharmonic couplings to the lattice modes, namely, the linear, $\alpha_{\mathbf{k}}q_{\mathbf{k}}$ and quadratic terms $\beta_{\mathbf{k}\mathbf{k}'}q_{\mathbf{k}}q_{\mathbf{k}'}$ (where $q_{\mathbf{k}}$ represents the normal coordinate

of mode \mathbf{k}). The VSCF calculations considered the quadratic coupling terms $\beta_{\mathbf{k}\mathbf{k}'}$ by evaluating the energy differences for the molecular vibrations with and without the occupation of a given lattice mode. A strictly linear dependence on ν is observed for a given normal mode of the lattice, as well as for the mean over all modes. It is therefore safe to assume that the same holds for the nondiagonal couplings, $\beta_{\mathbf{k}\mathbf{k}'}$. In essence, the observed linear dependence of dephasing with vibrational quantum numbers is consistent with expectations based on the interaction potential between iodine and argon.

Homogeneous dynamical dephasing, both dissipation ($1/T_1$) and pure dephasing ($1/T_2$), occurs through the scattering of phonons. Given the Debye limit of solid Ar of 65 cm^{-1} , dissipation of a quantum of molecular vibration of 200 cm^{-1} must be accompanied by the creation of at least three phonons. Pure dephasing occurs through the quasi-elastic scattering of phonons from the impurity and is most commonly diagnosed through temperature dependence studies [19,20]. Clearly, in the limit $T \rightarrow 0$, a finite dephasing rate must be reached. So, quite generally, we may expect:

$$\gamma = \gamma_0 + \gamma(T), \text{ where } \gamma_0 = \gamma(T \rightarrow 0). \quad (7)$$

For pure dephasing, two important limits are widely accepted for $\gamma(T)$ in solids. The scattering of acoustic phonons, through a generalized linear coupling, $\beta_{\mathbf{k}\mathbf{k}'}$ leads to a (T/T_D) [7] dependence assuming a Debye density of states [19,21,22]. For solid Ar, this would predict a 200 fold increase in $\gamma(T)$ for the experimental range of $T = 17\text{--}35 \text{ K}$. The absence of such a dramatic effect would imply that $\gamma_0 \gg \gamma(T)$ in the measured temperature range, i.e., dephasing due to scattering of acoustic phonons is negligible. Alternatively, the process may be driven through coupling to a particular coordinate, a pseudo-local mode (PLM), in which case an exponential temperature dependence given by the probability of occupation of the mode is to be expected [23,24]:

$$\gamma = \gamma_0 + \frac{1}{2\tau} \exp(-E_{PL}/k_B T). \quad (8)$$

The limited data, the T -dependent rates for the $\nu = 13, 14$ packet, fit this scheme, as shown in Fig. 9. The parameters for the curve are: $\gamma_0 = 0.237 \text{ ps}^{-1}$, $\tau = 0.25 \text{ ps}$, $E_{PL} = 98 \text{ K}$ (or $\omega_{PL} = 68 \text{ cm}^{-1}$). The implied pseudo-local mode is just outside the Debye edge, $E_D(\text{Ar}) = 93 \text{ K}$. The introduction of the impurity does generate such localized modes, modes which are intimately coupled to the molecule [4]. In this model, τ is interpreted as the local mode lifetime (the time it takes for the local mode to decay into acoustic

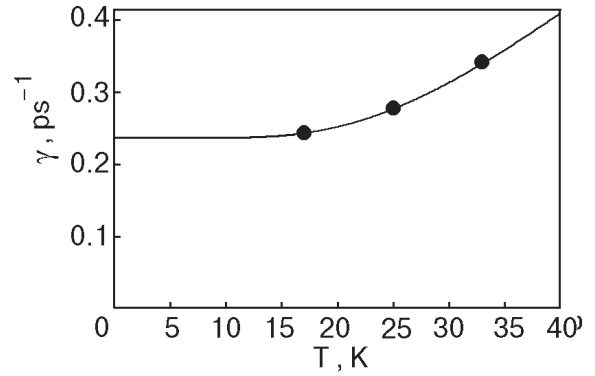


Fig. 9. The temperature dependence of measured dephasing rates (filled circles) and the curve for dephasing via a pseudo-local mode at the Debye edge (see Eq. (8)).

phonons) [24]. Evidently, the mode decays in half a period of its motion, what may be regarded as the fast exchange limit where Eq. (8) is applicable.

The absence of a measurable temperature dependence for the lower vibrations, and below $T = 17 \text{ K}$ in the case of $\nu = 13, 14$, implies that we are in a regime where γ_0 dominates. This limit may be determined by inhomogeneous broadening, due to lattice defects. While difficult to ascertain this possibility, inhomogeneous effects can in principle be eliminated through degenerate four-wave mixing measurements (photon echo) [25]. Given the elimination of inhomogeneous contributions, it is interesting to speculate as to what mechanism would control the residual dephasing, or Raman linewidth. The common assumption is that γ_0 will be determined by dissipation, since this appears to be a spontaneous process in contrast to dephasing which is usually defined to be stimulated via the scattering of thermal phonons. We can expect classical molecular dynamics to provide a useful estimate for vibrational relaxation, given the fairly well understood potentials of this system. To this end, we have carried out simulations, using reasonable potentials: Morse for I-I, Lennard-Jones for Ar-Ar and I-Ar. In a simulation box of 250 Ar atoms and a single I_2 molecule isolated in a divacancy, we calculate the rate of energy loss from trajectories propagated for 100 ps. At the classical temperature of 20 K, we estimate a vibrational relaxation time of 200 ps for $\nu = 5$ and 70 ps for $\nu = 15$. Thus, the classical estimates indicate rates of relaxation more than one order of magnitude smaller than what is observed experimentally for γ_0 . These results may well depend on the details of the assumed potentials, a systematic analysis of which has not been done. Pump-probe experiments which follow population dynamics, should provide a more definitive assessment of dissipation rates. We find the calculated

long $1/T_1$ times sensible. Moreover, since the relaxation is a multiphonon process, one would expect the classical limit to be an over-estimate for the rate. It would seem to us that a spontaneous three phonon process is less likely than pure dephasing at absolute zero, if recognized that in a strictly quantum world spontaneous processes are driven by quantum zero-point fluctuations [26]. If we allow for zero-point fluctuations in phonon modes, in the form of creation-annihilation events, then a natural mechanism for pure dephasing at 0 K would seem more plausible than dissipation driven by multiphonon fluctuations. We intend a more quantitative analysis of this distinction, since the issue is of relevance when control of decoherence is contemplated.

5. Conclusions

Through TRCARS experiments, we have been able to prepare and interrogate vibrational packets at vibrations as high as $v = 14$ in the model system of matrix isolated molecular iodine. This, to our knowledge, may be the first systematic study of its kind. The creation of vibrational coherences of large amplitude (up to $v = 14$), which is requisite for meaningful coherent control in condensed media, has been demonstrated. The coherences are long-lived, more than 100 vibrational periods at $v = 14$, much longer than necessary for most control targets of chemical nature. These time domain experiments have a higher spectral resolution than has been possible in frequency domain measurements. More importantly, the direct time-domain measurements allow detailed insights in the dephasing processes. Nevertheless, here, we have focused on the more robust features of the data.

The coherence decay time reduces from 16 ps near $v = 3$ to 2.5 ps near $v = 13$, showing a nearly linear dependence on vibrational quantum number.

The decoherence rates are a weak function of temperature for vibrations below $v = 10$, indicating that the process is controlled by the 0 K limit. We speculate on the nature of dephasing in this limit, with the conjecture that it will be driven by quantum zero-point fluctuations of the phonons.

A thermal contribution to dephasing is observed for packets prepared at $v = 13, 14$. The dependence is exponential, consistent with dephasing by a pseudo-local mode just outside the Debye edge of pure Ar. This mode decays into acoustic phonons in a half-period of motion.

Inhomogeneous dephasing due to vacancy point-defects has been identified by the quantitative agreement of the observable signal with an earlier theoretical prediction.

The above conclusions are derived from limited experimental scrutiny, because the signal degrades during the measurements. The origin of this decay is shown to be due to two-photon induced photodissociation. A more complete analysis of the breaking of the Ar cage, kinetics and dynamics of the process will be taken up elsewhere. Under the same irradiation conditions, photodissociation rates are much smaller in solid Kr; as such, they provide a more useful medium for systematic measurements. We have initiated such measurements.

Acknowledgments

This research was made possible through a grant from the USAFOSR (F49620-01-1-0449).

1. M. Karavitis, R. Zadoyan, and V.A. Apkarian, *J. Chem. Phys.* **114**, 4131 (2001).
2. S. Mukamel, *Principles of Nonlinear Optical Spectroscopy*, Oxford University Press, New York (1999).
3. J.C. Wright, *Intern. Rev. Phys. Chem.* **21**(2), 185 (2002).
4. Z. Bihary, M. Karavitis, R.B. Gerber, and V.A. Apkarian, *J. Chem. Phys.* **115**, 8006 (2001).
5. H. Dubost, *J. Low Temp. Phys.* **111**, 615 (1998).
6. M. Broquier, A. Cuisset, C. Crepin, H. Dubost, and J.P. Galaup, *J. Lumin.* **94**, 575 (2001); C. Crepin, M. Broquier, H. Dubost, J.P. Galaup, J.L. Le Gouet, and J.M. Ortega, *Phys. Rev. Lett.* **85**, 964 (2000).
7. W.F. Howard and L. Andrews, *J. Raman Spectr.* **2**, 442 (1974).
8. S. Maeda, T. Kamisuki, and Y. Adachi, *Adv. Nonlinear Spectrosc.* **30**, 807 (1999).
9. A.V. Benderskii; R. Zadoyan, and V.A. Apkarian, *J. Chem. Phys.* **107**, 8437 (1997).
10. M. Macler and M. Heaven, *Chem. Phys.* **151**, 219 (1991).
11. R. Zadoyan, Z. Li, C. Martens, P. Ashjian, and V.A. Apkarian, *Chem. Phys. Lett.* **218**, 504 (1994).
12. J. Helbing and M. Chergui, *J. Chem. Phys.* **115**, 6158 (2001).
13. P.B. Beeken, E.A. Hanson, and G.W. Flynn, *J. Chem. Phys.* **78**, 5892 (1983).
14. R. Bohling, J. Langen, and U. Schurath, *Chem. Phys.* **130**, 419 (1989).
15. D. Magde, *J. Chem. Phys.* **68**, 3717 (1978).
16. J. Almy, K. Kizer, R. Zadoyan, and V.A. Apkarian, *J. Phys. Chem.* **A104**, 3508 (2000).
17. J. Tellinghuisen, *J. Chem. Phys.* **76**, 4736 (1982).
18. Z. Li, R. Zadoyan, V.A. Apkarian, and C.C. Martens, *J. Phys. Chem.* **99**, 7453 (1995).
19. J.L. Skinner and D. Hsu, *J. Phys. Chem.* **90**, 4931 (1986); *Chem. Phys.* **128**, 35 (1988).
20. M.A. Krivoglaz and V.V. Hyzhnyakov, in: *Zero-Phonon Lines*, O. Sild and K. Haller (eds.), Springer-Verlag, Berlin (1988).
21. R.H. Silsbee, *Phys. Rev.* **128**, 1726 (1962).

22. D.E. McCumber, *J. Math. Phys.* **5**, 508 (1964); D.E. McCumber and M.D. Sturge, *J. Appl. Phys.* **34**, 1682 (1963).
23. C.B. Harris, *J. Chem. Phys.* **67**, 5607 (1977); C.B. Harris, R.M. Shelby, and P.A. Cornelius, *Phys. Rev. Lett.* **38**, 1415 (1977).
24. P. deBree and D.A. Wiersma, *J. Chem. Phys.* **70**, 790 (1979).
25. K.D. Rector and M.D. Fayer, *Int. Rev. Phys. Chem.* **17**, 261 (1998), and references therein.
26. D. Cohen, *J. Phys.* **A31**, 8199 (1998).